Generation of femtosecond dual pulses by a transverse standing wave in a volume holographic grating

Xiaoyan Wang (王晓燕), Xiaona Yan (阎晓娜)*, Kailong Jin (金凯龙), Ye Dai (戴 晔), Zuanming Jin (金钻明), Xihua Yang (杨希华), and Guohong Ma (马国宏)

Physics Department of Science College, Shanghai University, Shanghai 200444, China
**Corresponding author: xnyan@staff.shu.edu.cn*

Received April 10, 2019; accepted June 20, 2019; posted online September 4, 2019

Based on Kogelnik's coupled-wave theory, it is found that when a femtosecond pulse is incident on a transmitted volume holographic grating, two transverse standing waves along the grating vector direction will be generated inside the volume holographic grating (VHG). Due to field localization of two standing waves, they have two different velocities along the propagation depth. On the output plane of the VHG, femtosecond dual pulses are generated in both the diffracted and transmitted directions. Results show that the pulse interval is determined by the refractive index modulation and thickness of the grating, while the waveform of the dual pulses is independent of the grating parameters.

OCIS codes: 320.5540, 050.7330, 050.1940.
doi: 10.3788/COL201917.113201.

Femtosecond dual pulses, due to their short pulse duration and high spectral resolution, have found applications in various fields, such as femtosecond micromachining, ultrafast pump-probe spectroscopy, and coherent control of quantum states[1–4].

The common method to generate femtosecond dual pulses uses autocorrelators. However, due to material dispersion and absorption, the beam splitter needs to be as thin as 2 μm in some strict conditions, which significantly limits its practical applications. Later, Zhou's group proposed several schemes to generate femtosecond dual pulses based on diffraction of plane Dammann gratings[5–7]. Volume holographic gratings (VHGs), compared with plane gratings, have the advantages of high diffraction efficiency and strict Bragg selectivity. Based on these properties, our group generated femtosecond dual pulses in a VHG by adjusting refractive index modulation[8]. In this Letter, based on transverse standing-wave distribution in the VHG, we propose a new scheme to generate femtosecond dual pulses.

Using the general solutions of Kogelnik's coupled-wave equations[9], we found that when a femtosecond pulse is incident on the VHG, four waves are coupled out and coherently combine into two transverse standing waves along the grating vector direction. Due to field localization, two standing waves will propagate with two different velocities along the propagation depth; thus, with the increase of the depth in the VHG, two standing waves will separate from each other. On the output plane of the VHG, each standing wave is divided into a transmitted pulse and a diffracted pulse. Thus, dual pulses are output in both the transmitted and diffracted directions. It is found that the waveform of each diffracted pulse is independent of the VHG parameters, while the pulse interval between dual pulses depends on the grating thickness and refractive index modulation. Thus, interval modulated femtosecond dual pulses are generated.

Temporal- and frequency-domain diffractions of a femtosecond and nanosecond pulse by single-layer VHGs[10–18] and multi-layer VHGs[19–21] have been discussed earlier, but none of them touched on transverse standing-wave distribution in the VHG. Moreover, previous work on temporal diffraction of single-layer VHGs[10,11] found only one diffracted pulse, with a waveform that can be modulated by VHG parameters due to Bragg selectivity. However, in this Letter, on conditions when diffracted dual pulses emerge the waveform of each pulse is independent of the VHG parameters. Moreover, Refs. [8,11] acquired diffracted dual pulses, but the overmodulation effect is used to depict its physical origin. This means that the diffraction of a femtosecond pulse by the VHGs needs in-depth study.

The discussed VHG is a static unslanted phase grating whose grating planes are normal to the x axis, as shown in Fig. 1. The refractive index of the VHG is

$$n = n_0 + \Delta n \cos(Kx), \tag{1}$$

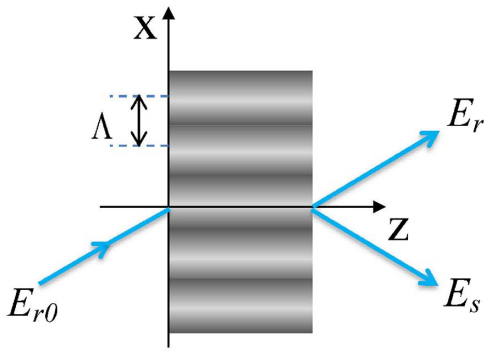

Fig. 1. Diffraction of a plane wave by a transmitted VHG.

where n_0 is the background refractive index of the VHG material; Δn is the refractive index modulation; grating vector $\boldsymbol{K}$ is parallel to the x axis, with wavenumber $K = 2\pi/\Lambda$ in which the grating period $\Lambda = \lambda_r/(2\sin\theta_r)$, with λ_r and θ_r being the Bragg wavelength and the angle outside the VHG, respectively.

A temporal femtosecond pulse is incident on the recorded VHG at Bragg angle θ_r,

$$e_{r0}(t) = \exp\left(-j\omega_0 t - \frac{t^2}{T^2}\right), \tag{2}$$

where $\omega_0 = 2\pi c/\lambda_0$ is the central angular frequency, with λ_0 as the central wavelength; T is related to the full width at half-maximum (FWHM) $\Delta\tau$ of the incident pulse by $T = \Delta\tau/2\sqrt{\ln 2}$.

By applying a Fourier transform on Eq. (2), we get

$$\begin{aligned} E_{r0}(\omega) &= \frac{1}{2\pi}\int_{-\infty}^{\infty} e_{r0}(t)\exp(j\omega t)\mathrm{d}t \\ &= \frac{T}{2\sqrt{\pi}}\exp\left[-\frac{T^2(\omega-\omega_0)^2}{4}\right]. \end{aligned} \tag{3}$$

According to Fourier optics, the incident femtosecond pulse can be assumed as a superposition of plane waves with different frequencies; the complex amplitude of each wave is represented by Eq. (3). Upon readout, each plane wave component couples out two plane waves with the same frequency inside the VHG, and the total field is

$$\begin{aligned} E(\omega,z,x) &= E'_r(\omega,z,x) + E'_s(\omega,z,x) \\ &= E_r(\omega,z)\exp(-j\boldsymbol{\rho}\cdot\boldsymbol{r}) \\ &\quad + E_s(\omega,z)\exp(-j\boldsymbol{\sigma}\cdot\boldsymbol{r}), \end{aligned} \tag{4}$$

where $E_r(\omega,z)$ and $E_s(\omega,z)$ are complex field amplitudes of the transmitted and diffracted waves, respectively; $\boldsymbol{\rho} = (k_x, k_z)$ and $\boldsymbol{\sigma} = (k_x - K, k_z)$ are the corresponding propagation vectors with $k_x = k\sin\theta$ and $k_z = k\cos\theta$, $k = \omega n_0/c$ is the wavenumber in crystal; θ is the readout angle inside the VHG and is determined by Snell's law $\sin\theta_r = n_0\sin\theta$. $\boldsymbol{\rho}$ and $\boldsymbol{\sigma}$ relate to the grating vector $\boldsymbol{K}$ by the relation $\boldsymbol{\sigma} = \boldsymbol{\rho} - \boldsymbol{K}$.

The total field in the VHG satisfies the scalar wave equation $\nabla^2 E + k^2 E = 0\,(k = \omega n/c)$. Considering the slowly varying envelope approximation, the coupled-wave equations describing the diffraction of a plane wave with frequency ω by a VHG are:

$$\begin{aligned} \frac{\mathrm{d}E_r(\omega,z)}{\mathrm{d}z} &= \frac{-j\kappa E_s(\omega,z)}{\cos\theta}, \\ \frac{\mathrm{d}E_s(\omega,z)}{\mathrm{d}z} + \frac{j\delta E_s(\omega,z)}{\cos\theta} &= \frac{-j\kappa E_r(\omega,z)}{\cos\theta}, \end{aligned} \tag{5}$$

where $\kappa = \omega\Delta n/2c$ is the coupling coefficient, c is the speed of light in vacuum, and $\delta = -\frac{cK^2}{2n_0}\left(\frac{1}{\omega} - \frac{1}{\omega_0}\right)$ is the Bragg deviation.

Assuming that the general solutions of Eq. (5) are[9]:

$$\begin{aligned} E_r(\omega,z) &= r_1\exp(j\gamma_1 z) + r_2\exp(j\gamma_2 z), \\ E_s(\omega,z) &= s_1\exp(j\gamma_1 z) + s_2\exp(j\gamma_2 z), \end{aligned} \tag{6}$$

where

$$\gamma_{1,2} = -\frac{\delta}{2\cos\theta_s} \pm \frac{1}{2}\sqrt{\left(\frac{\delta}{\cos\theta_s}\right)^2 + 4\frac{\kappa^2}{\cos\theta_s\cos\theta}}, \tag{7}$$

$$\begin{aligned} r_1 &= 1 - r_2 = \frac{\gamma_2}{\gamma_2 - \gamma_1}E_{r0}(\omega), \\ s_1 &= -s_2 = \frac{\kappa}{(\gamma_2 - \gamma_1)\cos\theta}E_{r0}(\omega), \end{aligned} \tag{8}$$

and θ_s is the diffraction angle in the VHG. Equation (7) shows that for all spectral components of the incident femtosecond pulse $\gamma_1 > 0$ and $\gamma_2 < 0$. Equations (7) and (8) show that r_i, s_i and $\gamma_i\,(i = 1, 2)$ are real numbers.

Combining Eqs. (6)–(8) with Eq. (4), the field and intensity of the transmission and diffraction of the VHG can be rewritten as

$$\begin{aligned} E'_r(\omega,z,x) &= [r_1\exp(-jq_{0z}^{(1)}z) + r_2\exp(-jq_{0z}^{(2)}z)] \\ &\quad \times \exp(-jq_{0x}x) = E_{r1} + E_{r2}, \\ E'_s(\omega,z,x) &= [s_1\exp(-jq_{0z}^{(1)}z) + s_2\exp(-jq_{0z}^{(2)}z)] \\ &\quad \times \exp[-j(q_{0x} - K)x] = E_{s1} + E_{s2}, \end{aligned} \tag{9}$$

$$I_i(t,z,x) = \left|\frac{1}{2\pi}\int_{-\infty}^{+\infty} E'_i(\omega,z,x)\exp(-j\omega t)\mathrm{d}\omega\right|^2, \quad i = r, s, \tag{10}$$

where $q_{0z}^{(1)} = k_z - \gamma_1$, $q_{0z}^{(2)} = k_z - \gamma_2$, and $q_{0x} = k_x$ are real functions representing the wave vector projections of the transmitted and diffracted waves on the z and x axes inside the VHG.

It is clearly seen from Eq. (9) that when a plane wave is incident on the VHG, four waves will be generated: the pair of waves E_{r1} and E_{r2} with wave vectors $\left(q_{0x}; q_{0z}^{(1,2)}\right)$ propagating in the transmitted direction, while the other pair of waves E_{s1} and E_{s2} with wave vectors $\left(q_{0x} - K; q_{0z}^{(1,2)}\right)$ propagating in the diffracted direction. Figure 2 shows a wave vector diagram of the four waves inside the VHG when a plane wave is incident on the VHG.

In the following, based on different combinations of wave fields E_{r1}, E_{r2}, E_{s1}, and E_{s2}, we will discuss the diffraction inside and outside the VHG. Note, except for special definitions, the simulated parameters are chosen as if VHG is recorded in a photorefractive $Fe{:}LiNbO_3$ crystal. To make a refractive index modulation of the VHG large enough, the optical axis of the crystal should be parallel to the grating vector when recording. The background refractive index of the crystal is $n_0 = 2.211$, and the refractive index modulation is $\Delta n = 1.25\times10^{-2}$; the grating

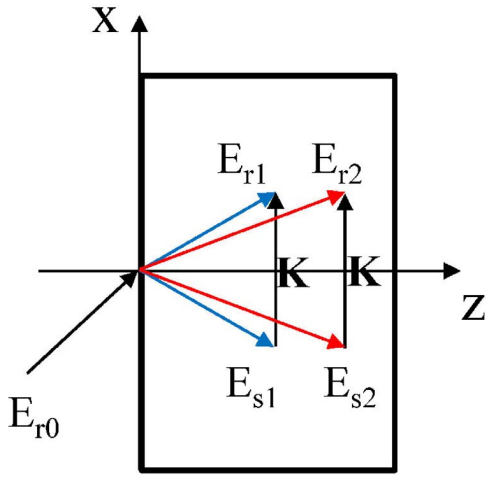

Fig. 2. Wave vector diagram inside the VHG with a plane wave reading out the VHG.

thickness $d = 6$ mm and period $\Lambda = 7.3$ μm; the central wavelength and duration of the incident femtosecond pulse are $\lambda_0 = 1.5$ μm and $\Delta\tau = 100$ fs, respectively.

In Eq. (9), by combining two fields with the same wave vector projection on the z axis together, we define two new spectral fields E_{rs1} and E_{rs2}:

$$\begin{aligned} E_{rs1}(\omega, z, x) &= E_{r1} + E_{s1} = \{r_1 \exp(-jq_{0x}x) \\ &\quad + s_1 \exp[-j(q_{0x} - K)x]\} \exp(-jq_{0z}^{(1)} z), \\ E_{rs2}(\omega, z, x) &= E_{r2} + E_{s2} = \{r_2 \exp(-jq_{0x}x) \\ &\quad + s_2 \exp[-j(q_{0x} - K)x]\} \exp(-jq_{0z}^{(2)} z). \end{aligned} \tag{11}$$

By applying an inverse Fourier transform on the sum of the four fields, the temporal total intensity inside the VHG is

$$I(t, z, x) = \left| \frac{1}{2\pi} \int_{-\infty}^{\infty} \left[E_{rs1}(\omega, z, x) + E_{rs2}(\omega, z, x) \right] \exp(-j\omega t) \mathrm{d}\omega \right|^2. \tag{12}$$

Figure 3 shows five diagrams to describe the evolutions of the total intensity with respect to x and time t when the propagation depths z are, respectively, 1, 2, 3, 3.4, and 4 mm. Note that when z is larger than 3 mm, for each depth z, there are two sets of transverse standing waves along the x axis, and they show strong spatial localization. The peaks of the first (right) set of standing waves are mainly localized in the lower refractive index layers of the VHG, while peaks of the second (left) set are localized in the higher refractive index layers. Each pulse in the standing waves propagates along a specific grating layer with a defined refractive index. The formation and location of the two transverse standing waves can be explained by Eq. (11).

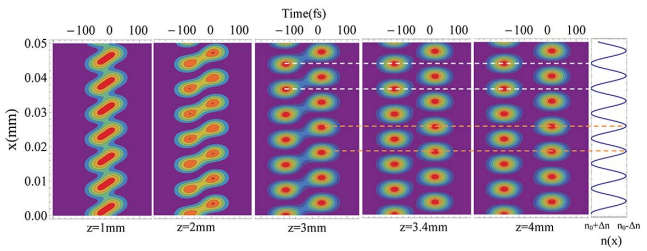

Fig. 3. Temporal total intensity inside the VHG when the propagation depth $z = 1, 2, 3, 3.4$, and 4 mm. The refractive index distribution of the VHG is also shown at the end of the diagram.

In Eq. (11), E_{rs1} includes a pair of transmitted and diffracted plane waves E_{r1} and E_{s1}, wave vectors of which have the same projections on the z axis, which means that the two plane waves propagate along the z axis with the same phase velocity. In addition, wave vector projections of the two plane waves on the x axis show an equal magnitude but opposite sign. As a result, the coherent superposition of the two fields E_{r1} and E_{s1} forms a transverse standing wave along the x axis, and the standing wave propagates along the z axis with a phase velocity determined by the wave vector projection $q_{0z}^{(1)}$. Likewise, coherent superposition of two other fields E_{r2} and E_{s2} forms another transverse standing wave that propagates along the z axis with a phase velocity determined by $q_{0z}^{(2)}$. When two standing waves represented by Eq. (11) are transformed into the time domain by Eq. (12), two temporal transverse standing waves along the x axis will emerge, just as what Fig. 3 shows.

Now based on Eq. (11), we depict the locations of the two transverse standing waves. Figure 4 shows that the intensity distributions of the two transmitted and two diffracted waves are the same; according to Eq. (8), we further have $-s_1 = s_2 = r_1 = r_2$. Moreover, for the central spectral component, $q_{0x} = 1/2K$. Substituting these

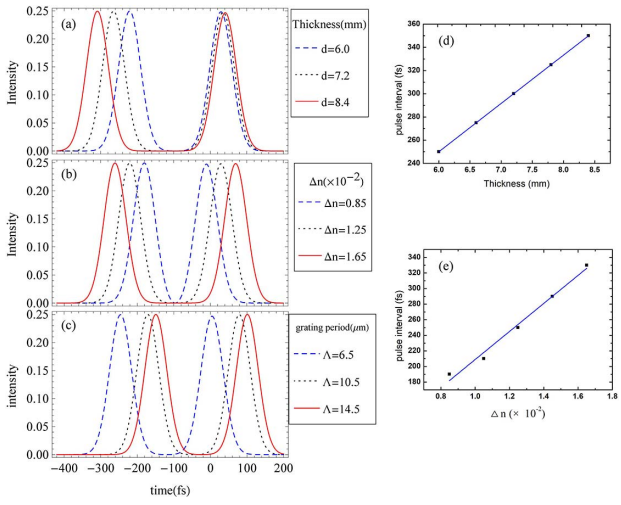

Fig. 4. Dependence of diffracted dual pulses on VHG parameters: (a) thickness, (b) refractive index modulation, and (c) period. Pulse interval with respect to (d) thickness and (e) refractive index modulation of the VHG.

values into Eq. (11), expressions of the two standing waves near the Bragg condition can be acquired:

$$E_{rs1} \propto -j2\sin\left(\frac{1}{2}Kx\right)\exp\left(-jq_{0z}^{(1)}z\right),$$
$$E_{rs2} \propto 2\cos\left(\frac{1}{2}Kx\right)\exp\left(-jq_{0z}^{(2)}z\right). \quad (13)$$

Accordingly, intensities of the two standing waves are, respectively,

$$I_{rs1} \propto 1-\cos(Kx), I_{rs2} \propto 1+\cos(Kx). \quad (14)$$

Comparing Eq. (14) with Eq. (1), we know that the two intensities have the same oscillation frequency as the refractive index of the VHG. The standing wave represented by I_{rs1} is out of phase with that of the refractive index; hence, peaks of the first standing wave are located on layers with a lower refractive index, while the standing wave represented by I_{rs2} is in phase with the refractive index; hence, peaks of the second standing wave are located on layers with a higher refractive index.

Two standing waves propagate along different grating layers; therefore, their propagating velocities are different. According to the group velocity expression, the velocities of the two standing waves along the z axis are

$$v_{gz}^{(1,2)} = \left.\frac{\partial\omega}{\partial q_{0z}^{(1,2)}}\right|_{\omega=\omega_0} = \frac{2c\cdot\cos\theta}{2n(\cos\theta)^2 \mp \Delta n}, \quad (15)$$

where "−" is chosen for the first standing wave, and "+" is for the second standing wave.

Equation (15) shows that the standing wave formed by E_{rs1} propagates faster than that of E_{rs2}. When z is small, two standing waves will overlap and coherently superpose along the z axis. When z is larger than 3 mm, the two standing waves will separate from each other.

On the output plane of the VHG, the faster standing wave arrives first. According to momentum conservation, it will break up into two pulses: the transmitted pulse propagating in the transmitted direction, and the diffracted pulse propagating in the diffracted direction. If the VHG is thick enough, the slower standing-wave pulse will arrive at the output plane with a certain time delay, where it will also break up into one transmitted pulse and one diffracted pulse. Thus, both transmission and diffraction will comprise femtosecond dual pulses.

Figures 4(a)–4(c) show diffracted dual pulses. It is seen that the duration and peak intensity of the diffracted dual pulses are similar and independent of the VHG parameters, while the pulse interval between the dual pulses is proportional to the thickness and refractive index modulation of the VHG, shown in Figs. 4(d) and 4(e).

In the following, we use the group velocity expression to deduce the relation between the pulse interval and VHG parameters.

Equation (15) shows that the two transverse standing waves have different group velocities along the z axis; as a result, a time delay will emerge when they output on the VHG with thickness d:

$$\Delta t = \frac{d}{v_{gz}^{(2)}} - \frac{d}{v_{gz}^{(1)}} = \frac{d\cdot\Delta n}{c\cos\theta}. \quad (16)$$

This time delay is the pulse interval between the dual pulses. Equation (16) shows that the pulse interval is linearly proportional to grating thickness and refractive index modulation, but independent of the grating period. The results are consistent with those of Fig. 4.

From above discussions, we know that by adjusting thickness and refractive index modulation of the VHG, we can generate femtosecond dual pulses with a variable pulse interval.

Figure 4 shows that the duration and peak intensity of the diffracted dual pulses are independent of the VHG parameters, while in Refs. [10,11], the diffraction includes only one pulse, the duration and peak intensity of which are strongly affected by the VHG parameters. In the following, we will give explanations of these phenomena and discuss the conditions to diffract out one or dual pulses.

According to former discussions, we know that the dual pulses originate from two separate transverse standing waves, so waveforms of the diffracted dual pulses are determined by standing waves' waveforms. When the thickness or refractive index modulation of the VHG is large enough, the two transverse standing waves will separate. In this case, each standing wave propagates along specific VHG layers, just as it propagates along a uniform medium, therefore increasing VHG thickness will not affect waveforms of the two standing waves and also have no effect on the waveforms of diffracted dual pulses. When the refractive index modulation changes, according to Eq. (15), velocities of two standing waves will change, while according to Eq. (14) localization remains unchanged. Thus the waveforms of the two standing waves and diffracted dual pulses are not affected by the refractive index modulation of the VHG.

Figure 5 shows that the grating period determines the oscillation period of the two standing waves along the x axis, while waveforms of the two standing waves along the time axis are unchanged. The dual pulses we discussed

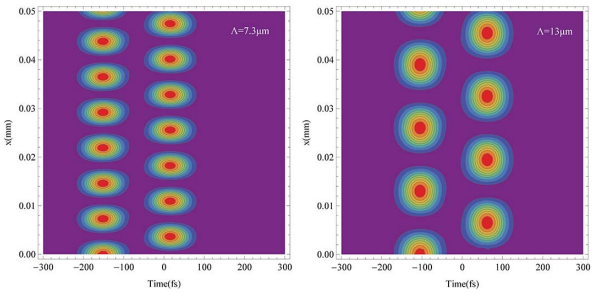

Fig. 5. Temporal total intensity inside the VHG when the grating periods are 7.3 and 13 μm.

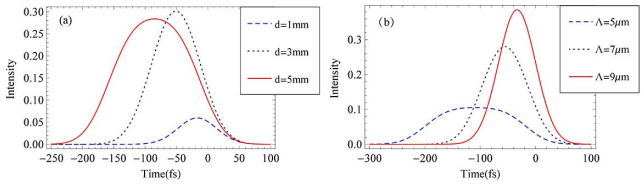

Fig. 6. Temporal diffracted intensity under a smaller $\Delta n \cdot d$ and grating period: (a) refractive index modulation $\Delta n = 1.25 \times 10^{-4}$; (b) $d = 3$ mm and $\Delta n = 1.25 \times 10^{-4}$.

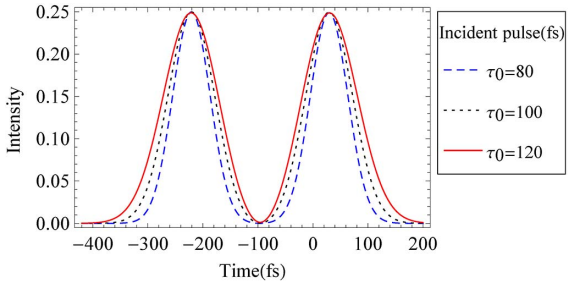

Fig. 7. Dependence of temporal diffracted intensity on the duration of incident femtosecond pulses.

in Fig. 5(c) are along the time axis, so the waveforms are independent of the grating period.

When the refractive index modulation or thickness of the VHG decreases, according to Eq. (16), the pulse interval will decrease as well. If the pulse interval is smaller than the duration of each diffracted pulse, the diffracted dual pulses will overlap and coherently superpose. In this case, the diffracted dual pulses may converge into one pulse. Figure 6 further shows that the duration and peak intensity of the diffracted one pulse can be modulated by VHG parameters. The evolutions are consistent with those in Refs. [10,11] and can be explained by VHG Bragg selectivity. Therefore, to observe the pulse splitting or dual pulses in the diffraction of the VHG, products of refractive index modulation and thickness of the VHG must be large enough.

Figure 4 shows that the durations of the diffracted dual pulses are independent of VHG parameters. Figure 7 shows that they can be modulated by the duration of the incident femtosecond pulse. Note that the duration of each diffracted pulse is the same as that of the incident pulse.

Actually, as the femtosecond pulse is incident on the VHG, the dispersion of the material will have an influence on the diffraction. However, we do not consider it here. The reason is that, according to the discussions of Fig. 7 and Eq. (16), the dispersion will affect the duration of each diffracted pulse, but have no effect on the emergence and pulse interval of the diffracted femtosecond dual pulses, in which we are interested here.

In conclusion, diffraction-induced pulse splitting in a VHG and its underlying physical mechanisms are discussed. It is found that when a temporal Gaussian femtosecond pulse is incident on the transmitted VHG, four pulses are generated, which further combine into two transverse standing waves inside the VHG. Spatial localization of the two transverse standing waves in the VHG results in a different longitudinal group velocity. On the output plane, both diffraction and transmission include dual pulses with a pulse interval determined by the thickness and refractive index modulation of the VHG, while pulse waveforms are not affected by the VHG parameters.

This work was partly supported by the National Natural Science Foundation of China (Nos. 61735010, 11674213, 11574195, and 11774220).

References

1. H. Wang, J. Song, Q. Li, X. Zeng, and Y. Dai, J. Phys. D **51**, 155101 (2018).
2. Z. Luo, C. Wang, X. Dong, and J. Duan, Chin. Opt. Lett. **16**, 031401 (2018).
3. C. Daniel, J. Full, L. González, C. Lupulescu, J. Manz, A. Merli, S. Vajda, and L. Wöste, Science **299**, 536 (2003).
4. S. Iwai, Y. Ishige, S. Tanaka, Y. Okimoto, Y. Yokura, and H. Okamoto, Phys. Rev. Lett. **96**, 057403 (2006).
5. E. Dai, C. Zhou, and G. Li, Opt. Express **13**, 6145 (2005).
6. J. Zheng, C. Zhou, and E. Dai, J. Opt. Soc. Am. B **24**, 979 (2007).
7. T. Wu, C. Zhou, J. Zheng, J. Feng, H. Cao, L. Zhu, and W. Jia, Appl. Opt. **49**, 4506 (2010).
8. X. Yan, Y. Dai, L. Gao, Y. Chen, X. Yang, and G. Ma, Opt. Express **21**, 7560 (2013).
9. H. Kogelnik, Bell Syst. Tech. J. **48**, 2909 (1969).
10. X. Yan, B. Yang, and B. Yu, Optik **115**, 512 (2004).
11. Y. Yi, D. Liu, and H. Liu, J. Opt. **13**, 035701 (2011).
12. Y. Ding, D. D. Nolte, and Z. Zheng, J. Opt. Soc. Am. B **15**, 2763 (1998).
13. C. Wang, L. Liu, A. Yan, D. Liu, D. Li, and W. Qu, J. Opt. Soc. Am. A **23**, 3191 (2006).
14. M. P. Hernández-Garay, O. Martínez-Matos, J. G. Izquierdo, M. L. Calvo, P. Vaveliuk, P. Cheben, and L. Bañares, Opt. Express **19**, 1516 (2011).
15. T. Brixner and G. Gerber, Opt. Lett. **26**, 557 (2001).
16. M. Efimov, L. B. Glebov, and V. I. Smirnov, Opt. Lett. **25**, 1693 (2000).
17. L. A. Siiman, J. Lumeau, L. Canioni, and L. B. Glebov, Opt. Lett. **34**, 2572 (2009).
18. B. Xiong, F. Gao, X. Zhang, and X. Yuan, Chin. Opt. Lett. **17**, 040501 (2019).
19. A. Yan, L. Liu, Y. Zhi, D. Liu, and J. Sun, J. Opt. Soc. Am. A **26**, 135 (2009).
20. A. Yan, L. Liu, L. Wang, D. Liu, J. Sun, and L. Wan, Appl. Phys. B **96**, 71 (2009).
21. X. Yan, L. Gao, X. Yang Dai, Y. Chen, and G. Ma, Opt. Express **22**, 26128 (2014).